

# UniTracker: Learning Universal Whole-Body Motion Tracker for Humanoid Robots

Kangning Yin<sup>1,4\*</sup>, Weishuai Zeng<sup>2,4\*</sup>, Ke Fan<sup>1,4</sup>, Zirui Wang<sup>3,4</sup>, Qiang Zhang<sup>5</sup>,  
Zheng Tian<sup>6</sup>, Jingbo Wang<sup>4</sup>, Jiangmiao Pang<sup>4</sup>, Weinan Zhang<sup>1,4</sup>

<sup>1</sup>Shanghai Jiao Tong University, <sup>2</sup>Peking University, <sup>3</sup>Zhejiang University

<sup>4</sup>Shanghai Artificial Intelligence Laboratory

<sup>5</sup>The Hong Kong University of Science and Technology (Guangzhou) <sup>6</sup>ShanghaiTech University

<https://yinkangning0124.github.io/Humanoid-UniTracker/>

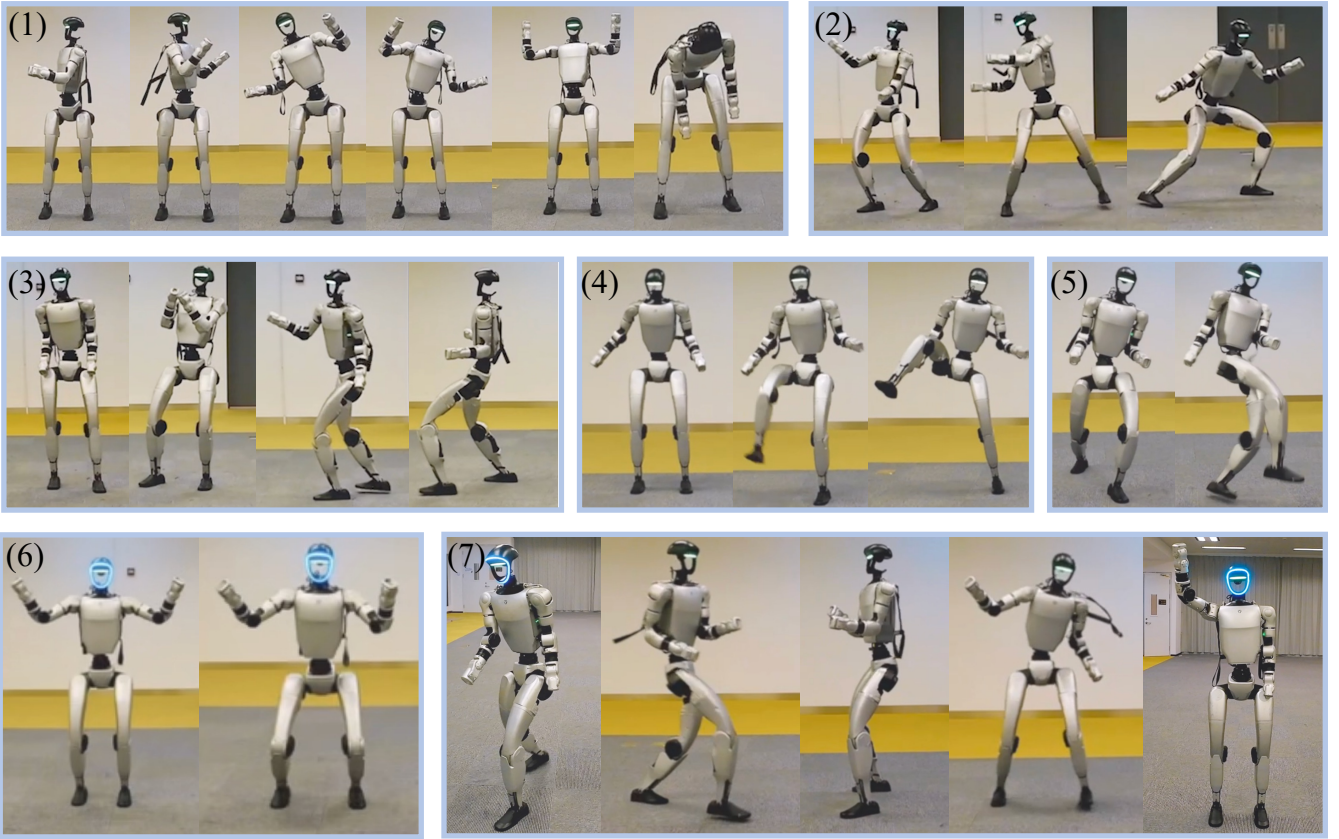


Fig. 1: We deploy our UniTracker on a real humanoid robot, enabling it to perform a diverse range of motions, including (1)stretching, (2)traditional Chinese martial arts, (3)dancing, (4)high kicks, (5)ball-kicking, (6)squatting, and (7)various other common motions.

**Abstract**—Humanoid robots must achieve diverse, robust, and generalizable whole-body control to operate effectively in complex, human-centric environments. However, existing methods, particularly those based on teacher-student frameworks often suffer from a loss of motion diversity during policy distillation and exhibit limited generalization to unseen behaviors. In this work, we present UniTracker, a simplified yet powerful framework that integrates a Conditional Variational Autoencoder (CVAE) into the student policy to explicitly model the latent diversity of human motion. By leveraging a learned CVAE prior, our method enables the student to retain expressive

motion characteristics while improving robustness and adaptability under partial observations. The result is a single policy capable of tracking a wide spectrum of whole-body motions with high fidelity and stability. Comprehensive experiments in both simulation and real-world deployments demonstrate that UniTracker significantly outperforms MLP-based DAGger baselines in motion quality, generalization to unseen references, and deployment robustness, offering a practical and scalable solution for expressive humanoid control.

## I. INTRODUCTION

Humanoid robots have garnered growing interest in the robotics community for their human-like morphology, which equips them with the potential to perform a wide range of tasks traditionally carried out by humans. To function effectively in real-world, human-centric environments, these robots must exhibit not only physical versatility but also robust and expressive motor control. Among the key enablers of such capabilities is whole-body control, which coordinates multiple joints and limbs to perform complex tasks while ensuring stability, adaptability, and energy efficiency.

Within this broader category, whole-body motion tracking plays a crucial role. It involves reproducing rich human motions, such as walking, kicking, turning, and dancing, based on reference trajectories from demonstrations or motion datasets. Unlike general task-driven control, tracking requires precise alignment with reference poses while maintaining robustness under real-world constraints such as sensor noise, partial observability, and actuation delay. This makes the problem especially challenging, as it demands both fidelity and stability in high-dimensional action spaces.

Recent research has explored various control interfaces tailored to whole-body motion tracking. These can be broadly categorized into dense and sparse control signals. Dense signals, such as teleoperation [1–6], offline motion datasets [7–12], and video-based motion estimation [13, 14], provide rich trajectory-level information. In contrast, sparse signals such as high-level task commands and VR-based guidance [15, 16] offer minimal information and often lead to reduced motion quality. In this work, we focus on universal whole-body tracking, where the input is a reference motion sequence and the goal is to track it robustly and expressively using a single policy.

A widely adopted approach is the teacher-student framework, where a teacher policy is trained with privileged observations to track the reference motion with high accuracy. The student policy then learns to mimic the teacher using only deployable observations. While effective in principle, existing student training methods—particularly those based on standard DAgger [17] often converge to averaged behaviors, losing the richness of the original motions. Moreover, these methods struggle to generalize to unseen motion sequences.

To address this limitation, we propose UniTracker, a unified and expressive whole-body tracking framework that introduces a Conditional Variational Autoencoder (CVAE) into the student policy. By explicitly modeling a structured latent space conditioned on future motion references, the policy learns to generate diverse and high-fidelity behaviors even under partial observations. From a probabilistic perspective, the latent variable captures ambiguity in the mapping from observations to actions, enabling the policy to approximate a distribution over plausible motor behaviors rather than collapsing to a single deterministic output.

Unlike prior works that directly include reference signals into the policy input, our approach encourages semantic abstraction by guiding behavior generation through latent

intention modeling. We further demonstrate that design choices such as residual KL formulation, latent dimension, and future window size significantly influence both training stability and downstream performance. Our training dataset is derived from the PHC-filtered AMASS corpus, which removes overly aggressive motions and improves real-world policy viability.

UniTracker is evaluated extensively in both simulation and real-world settings. Experiments on a 29-DoF Unitree G1 humanoid show that our policy can track 8k motions, including highly dynamic ones with a single network. Compared to strong teacher-student baselines without CVAE, UniTracker achieves better tracking accuracy, motion smoothness, and generalization. Furthermore, we demonstrate its application to text-driven motion generation and video-based motion estimation, where the policy successfully executes motions generated from external inputs not seen during training.

Our main contributions are summarized as follows: i) **Diversity-aware policy via CVAE modeling:** We introduce a Conditional Variational Autoencoder (CVAE) into the student policy to explicitly capture the distributional characteristics of human motions, allowing the policy to generate diverse and expressive behaviors under partial observations. ii) **Improved generalization to unseen motions:** By modeling motion diversity in a structured latent space, our approach enables the policy to generalize effectively to out-of-distribution motions, outperforming conventional DAgger-based methods. iii) **Robust real-world tracking with a single universal policy:** We demonstrate that our approach enables a humanoid robot to robustly track thousands of diverse human motions using a single policy, with successful deployment in both simulation and the real world.

## II. METHOD

### A. Problem Formulation

We formulate the problem of humanoid robot whole-body motion tracking as a goal-conditioned reinforcement learning (RL) task, where a policy  $\pi$  is trained to track reference motions at the whole-body level. The state  $s_t$  comprises the robot’s proprioceptive information  $s_t^p$  and the goal  $s_t^g$  which specifies the target state for all body parts. The reward function  $r_t = R(s_t^p, s_t^g)$ , defined in terms of the agent’s proprioception and goal state, yields dense signals to guide policy optimization. To better focus on motion tracking at the whole-body level, we fix the wrist joints of our 29-degree-of-freedom (DoF) Unitree G1 robot [18], reducing the action space to 23 dimensions. The action  $a_t \in \mathbb{R}^{23}$  specifies target joint positions, which are executed via a PD controller to actuate the robot. For policy optimization, we employ Proximal Policy Optimization (PPO) [19] to maximize the expected cumulative discounted reward  $\mathbb{E} \left[ \sum_{t=1}^T \gamma^{t-1} r_t \right]$ .

This setup raises two critical questions in developing a universal yet robust humanoid robot motion tracking policy: 1) how to maximize the policy’s expressiveness to track a diverse range of motions and 2) how to minimize the sim-to-real performance degradation caused by the dynamic mismatch between simulation and the real world.

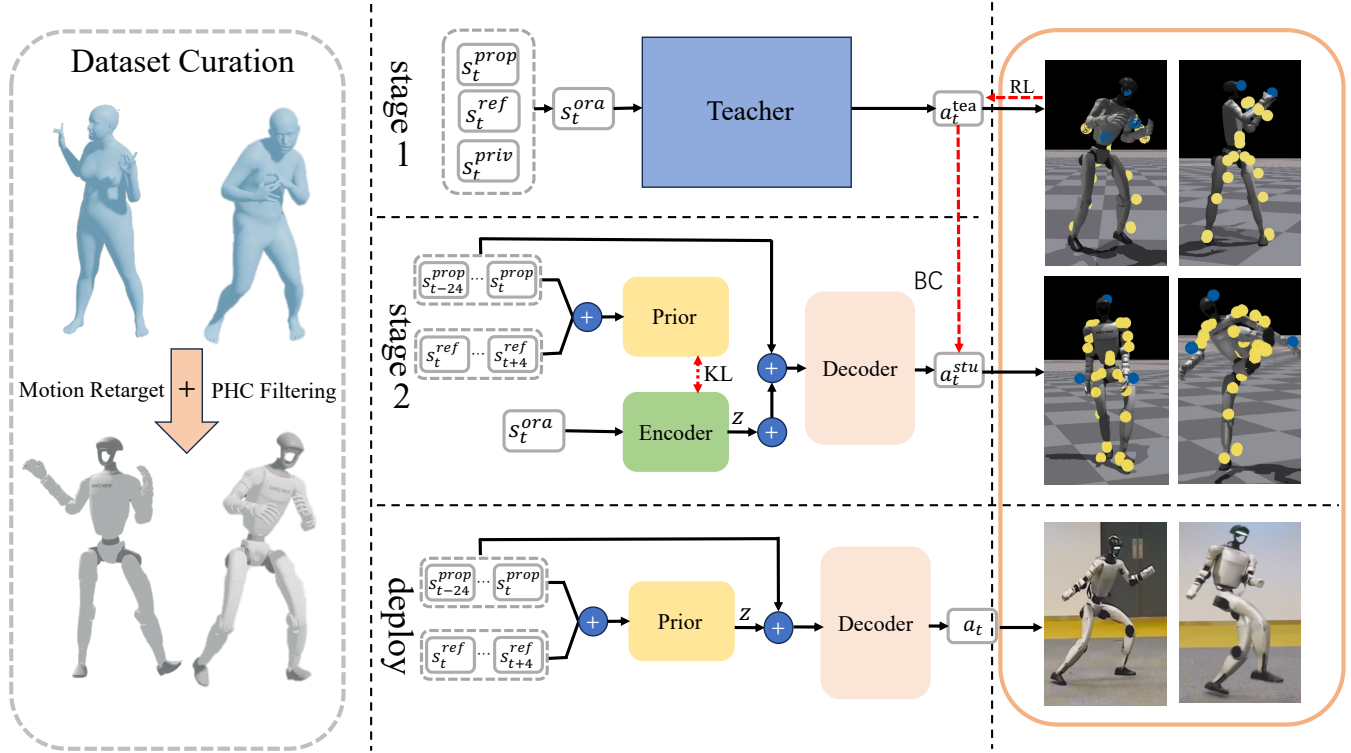


Fig. 2: **An overview of UniTracker:** In Stage 1, we train a teacher policy using oracle states via goal-conditioned reinforcement learning. In Stage 2, we distill the policy into a deployable form using a CVAE-based DAGger framework. In Stage 3, we deploy the policy using the CVAE prior and decoder for execution under partial observations. The training dataset is derived from the AMASS dataset, filtered by PHC to remove physically infeasible motions.

UniTracker addresses these challenges through a CVAE-based two stage training pipeline. First, we train a perturbation-free oracle policy in simulation using filtered reference motions retargeted from large-scale human motion dataset. Second, we distill the oracle policy into a hierarchical controller via a Conditional Variational Autoencoder (CVAE). The resulting universal whole-body motion tracker (UniTracker) is shown in Figure 2.

The remainder of this section is structured as follows. First, we describe the curation of a high-quality, feasible humanoid robot motion dataset for policy training in Section II-B and then detail the training of the oracle policy in simulation which attempts to maximize the expressiveness of our motion tracker in Section II-C. Further we explain the distillation of the oracle policy using CVAE in Section II-D

### B. Humanoid Motion Dataset Curation

A large-scale humanoid motion dataset serves as fuel for training a universal motion tracker. Our dataset is primarily derived from the publicly available AMASS [20] dataset, filtered to exclude interactions and sequences shorter than 10 frames. This yields a final training set of 11,313 human motions, represented using the SMPL [21] parameters. The SMPL model parameterizes the human body through shape parameters  $\beta \in \mathbb{R}^{10}$ , pose parameters  $\theta \in \mathbb{R}^{24 \times 3}$  and root translation  $p \in \mathbb{R}^3$ .  $S$  denotes the SMPL function, where  $S(\beta, \theta, p) : \mathbb{R}^{\beta, \theta, p} \rightarrow \mathbb{R}^{6980 \times 3}$  maps the SMPL parameters to the positions of vertices of a triangular human mesh.

To bridge the embodiment gap between SMPL human model and humanoid robots, we employ a two-stage retargeting approach inspired by H2O [4]. First, we carefully select 16 corresponding body links and optimize the shape parameter  $\beta'$  for humanoid robots by minimizing the distances between selected links in the rest pose. Second, leveraging the optimized  $\beta'$  alongside the original pose  $\theta$  and translation  $p$  from dataset, we perform gradient descent over the humanoid robot’s root translation, root orientation and joint positions to minimize the distances between selected links throughout the whole sequence. Additional regularization terms are added to avoid aggressive behaviors and ensure temporal smoothness.

### C. Oracle Policy Training in Simulation

**Oracle State Space Design.** We train an oracle motion tracking policy  $\pi^{oracle}(a_t | s_t^{p-oracle}, s_t^{g-oracle})$  with all the state information accessible in simulators. The proprioception is defined as  $s_t^{p-oracle} \triangleq [p_t, q_t, \theta_t, \dot{p}_t, \dot{q}_t, \omega_t, a_{t-1}]$ , which contains the humanoid rigid-body position  $p_t$ , orientation  $\theta_t$ , linear velocity  $\dot{p}_t$ , angular velocity  $\omega_t$ , joint position  $q_t$ , joint velocity  $\dot{q}_t$  and previous action  $a_{t-1}$ . The goal state is defined as  $s_t^{g-oracle} \triangleq [\hat{p}_{t+1} - p_t, \hat{q}_{t+1} - q_t, \hat{\theta}_{t+1} \ominus \theta_t, \hat{v}_{t+1} - v_t, \hat{\omega}_{t+1} - \omega_t, \hat{p}_{t+1} - p_t^{root}, \hat{\theta}_{t+1} \ominus \theta_t^{root}]$ , which contains the one-frame difference between the reference pose  $(\hat{p}_{t+1}, \hat{q}_{t+1}, \hat{\theta}_{t+1}, \hat{v}_{t+1}, \hat{\omega}_{t+1})$  and the current pose.  $p_t^{root}$  refers to the root translation and  $\theta_t^{root}$  refers to the root orientation of the current pose. All these states are rotated to the local coordinate of the current pose.

Methods	All AMASS Train Dataset				Successful AMASS Train Dataset		
	SR $\uparrow$	MPKPE $\downarrow$	Vel-Dist $\downarrow$	Acc-Dist $\downarrow$	MPKPE $\downarrow$	Vel-Dist $\downarrow$	Acc-Dist $\downarrow$
(a) Compare with Baselines							
Dagger without CVAE	88.21	84.79	5.60	2.97	84.70	5.03	2.41
Train from Scratch	58.32	145.59	12.35	10.11	139.77	11.92	10.04
Ours	<b>91.83</b>	<b>82.62</b>	<b>4.27</b>	<b>1.83</b>	<b>78.95</b>	<b>3.65</b>	<b>1.39</b>
(b) Ablation with Architecture Design							
Actor with Explicit Reference	88.29	85.31	5.76	3.03	84.96	4.58	2.15
Actor without Explicit Reference	<b>91.83</b>	<b>82.62</b>	<b>4.27</b>	<b>1.83</b>	<b>78.95</b>	<b>3.65</b>	<b>1.39</b>
(c) Ablation with KL Residual							
KL without Residual	85.49	91.24	6.02	4.68	90.79	6.01	4.23
KL with Residual	<b>91.83</b>	<b>82.62</b>	<b>4.27</b>	<b>1.83</b>	<b>78.95</b>	<b>3.65</b>	<b>1.39</b>
(d) Ablation with KL Coefficient							
KL Coef = 1.0	81.18	97.23	7.75	6.04	96.53	5.39	2.41
KL Coef = 0.1	<b>91.83</b>	<b>82.62</b>	<b>4.27</b>	<b>1.83</b>	<b>78.95</b>	<b>3.65</b>	<b>1.39</b>
KL Coef = 0.01	86.10	89.88	7.99	5.47	88.01	5.23	2.37
KL Coef = 0.001	80.55	105.56	9.21	7.98	104.63	5.38	2.40
(e) Ablation with Future Window Size							
Window Size = 1	90.77	85.98	5.20	3.12	85.00	4.79	2.91
Window Size = 5	<b>91.83</b>	<b>82.62</b>	<b>4.27</b>	<b>1.83</b>	<b>78.95</b>	<b>3.65</b>	<b>1.39</b>
Window Size = 10	91.28	<b>82.14</b>	4.77	1.95	<b>78.78</b>	3.90	1.87
Window Size = 20	90.29	82.96	5.01	1.78	80.24	4.33	1.48
(f) Ablation with Latent Dimension							
Latent Dimension = 32	88.82	87.25	4.79	2.36	86.52	4.67	2.21
Latent Dimension = 64	<b>91.83</b>	<b>82.62</b>	4.27	<b>1.83</b>	<b>78.95</b>	<b>3.65</b>	<b>1.39</b>
Latent Dimension = 128	90.54	83.75	4.46	2.14	82.92	4.45	2.08
Latent Dimension = 256	90.72	83.99	<b>4.21</b>	1.97	83.71	4.19	1.77
(g) Analysis of CVAE diversity							
Decoder with Stochastic Latent	91.77	83.21	4.59	1.82	79.07	3.72	<b>1.33</b>
Decoder with Deterministic Latent	<b>91.83</b>	<b>82.62</b>	<b>4.27</b>	<b>1.83</b>	<b>78.95</b>	<b>3.65</b>	1.39

TABLE I: **Baselines Comparison and Ablation Studies** We compare our method with two baseline approaches and observe that it consistently outperforms both. Additionally, we conduct ablation studies on architectural design, KL residuals, KL coefficient, future window size, and latent dimensionality. Finally, we analyze the diversity of CVAE comparing the stochastic latent and the deterministic latent. The final configuration is selected based on the best overall performance observed across these settings.

**Reward Design.** We formulate the reward  $r_t$  as a weighted sum of three components: 1) task rewards for motion tracking, 2) regularization, and 3) penalty, detailed in Table III. We apply curriculum learning to the regularization terms and penalty terms such that the policy could better focus on the motion tracking task itself and gradually take the penalty and regularization into account for more reasonable behaviors.

**Early Termination and Reference State Initialization.** In the early stage of training, the agent is prone to falling, resulting in the collection of invalid data that hinders effective learning. To address this issue, we follow prior works [22, 23] and introduce two early termination conditions: 1) orientation: the projected gravity on x or y axis exceeds 0.8; 2) tracking tolerance: the average link distance between the robot and reference motions is further than 0.5m. Proper task initialization is also crucial for RL training. We employ the Reference State Initialization [9, 22] framework, where the starting point of the reference motion is randomly sampled

for the policy to track. The robot’s initial state, including the root position, orientation, linear and angular velocities, as well as joint positions and velocities, is then derived from the corresponding reference pose. This initialization strategy substantially enhances motion tracking training by enabling the policy to learn different motions phases in parallel, rather being constrained to a sequential learning process.

**Domain Randomization.** Domain randomization has been proved to be a critical source of robustness and generalization for successful sim-to-real transfer [4, 6, 11]. Existing domain randomization terms can be broadly categorized into two classes: asset property randomization and environmental dynamic randomization. Asset property randomization, focusing on parameters such as friction coefficients, center of mass offsets, and link masses, aims to prevent the policy from overfitting to a specific asset configuration. In contrast, environmental dynamic randomization, focusing on PD gains, applied torques, or other external perturbations (e.g., pushing

the robot), introduces dynamic variations to simulate the environmental uncertainties encountered during real-world deployment. While previous works typically apply both forms of randomization concurrently throughout training, we propose decoupling them to better balance the tradeoff between motion tracking expressiveness and robustness. Hence, in the first stage, we exclusively randomize asset properties to maximize the policy's ability to accurately track diverse motions. This approach not only builds an upper bound for subsequent policies but also yields a proxy agent capable of generating high-quality action signals in simulators.

#### D. Hierarchical Controller via Online Distillation

**Deployable State Space Design.** Since certain privileged information in the oracle state space is unavailable in real-world deployment, we define a deployable state space based on data accessible on humanoid robots. The proprioception is defined as  $s_t^{p-deploy} \triangleq [q_t - 25:t, \dot{q}_t - 25:t, w_t^{root} - 25:t, g_t - 25:t, a_{t-25:t-1}]$  where  $q_t$  and  $\dot{q}_t$  denote joint positions and velocities,  $w_t^{root}$  refers to the root angular velocity,  $g_t$  is the gravity vector and  $a_{t-1}$  is the previous action. These terms are stacked over the past 25 steps to form the proprioceptive input. The goal state is defined as  $s_t^{g-deploy} \triangleq [\hat{h}_{t+1}, \hat{\theta}_{t+1}^{root} \ominus \theta_{t+1}^{root}, \hat{v}_{t+1}^{root}, \hat{w}_{t+1}^{root} - w_t^{root}, \hat{p}_{t+1} - \hat{p}_{t+1}^{root}]$ , where  $\hat{h}_{t+1}$  is the reference pose height,  $\hat{\theta}_{t+1}^{root}$  and  $\theta_{t+1}^{root}$  are the reference and current root orientations,  $\hat{v}_{t+1}^{root}$  and  $\hat{w}_{t+1}^{root}$  are the reference root linear and angular velocities,  $w_t^{root}$  is the current root angular velocity,  $\hat{p}_{t+1}$  and  $\hat{p}_{t+1}^{root}$  are the reference rigid body and root positions. The first four terms are rotated into the current pose's local coordinate while the last term is rotated into the reference pose's local frame.

**Modeling Diversity with CVAE** Our target is to obtain a deployable policy  $\pi^{deploy}(a_t | s_t^{p-deploy}, s_t^{g-deploy})$  which maintains the expressiveness of the oracle policy to the maximum. Given the deployable state space is partial and may lead to motion ambiguity, We model the deployable policy as a conditional variational autoencoder (CVAE) to model the diversity. Specifically, we have a variational encoder  $\varepsilon(z_t | s_t^{p-oracle}, s_t^{g-oracle})$  that computes the latent code distribution based on the same observation with the teacher policy, a decoder  $D(a_t | s_t^{p-deploy}, z_t)$  that produces action. We employ a learned conditional prior  $\rho(z_t | s_t^{p-deploy}, s_t^{g-deploy})$  following prior works which allows the model to learn different distributions based on proprioception. Using the evidence lower bound, we have the objective function as:

$$\log P(a_t | s_t^{p-d}, s_t^{g-d}) \geq E_{\varepsilon(z_t | s_t^{p-o}, s_t^{g-o})} [\log D(a_t | s_t^{p-d}, z_t) - D_{KL}(\varepsilon(z_t | s_t^{p-o}, s_t^{g-o}) || \rho(z_t | s_t^{p-d}, s_t^{g-d}))]$$

where the prior, encoder and decoder are all modeled as diagonal Gaussian distribution. Following prior works, we

model the encoder as a residual to the prior and have:

$$\begin{aligned} \rho(z_t | s_t^{p-d}, s_t^{g-d}) &= N(\mu^\rho(s_t^{p-d}, s_t^{g-d}), \sigma^\rho(s_t^{p-d}, s_t^{g-d})) \\ \varepsilon(z_t | s_t^{p-o}, s_t^{g-o}) &= N(\mu^\rho(s_t^{p-d}, s_t^{g-d}) + \mu^\varepsilon(s_t^{p-o}, s_t^{g-o}), \\ &\quad \sigma^\varepsilon(s_t^{p-o}, s_t^{g-o})) \\ D(a_t | s_t^{p-d}, z_t) &= N(\mu^D(s_t^{p-d}, z_t), \sigma^D(s_t^{p-d}, z_t)) \end{aligned}$$

To optimize the loss function, we use the action supervision signal provided by the oracle policy and learn the deployable policy in an online distillation fashion. The loss function derived from the objective above can be formulated as:

$$L = L_{action} + \beta L_{KL}$$

where  $L_{action} = ||a_t^{deploy} - a_t^{oracle}||_2^2$  and  $L_{KL}$  is the KL divergence between the prior and encoder.

### III. EXPERIMENT

#### A. Experiment Setup

We evaluate UniTracker in both simulated and real-world environments. In simulation, policies are trained using Isaac-Gym [24] with 8192 parallel environments under domain randomization [25]. The training data is derived from the AMASS dataset [20] and filtered by PHC [23]. We further validate our approach through sim-to-sim transfer by deploying the trained policies in MuJoCo, and conduct extensive ablation and comparative studies. Performance is assessed using four key metrics: Success Rate (SR), Mean Per Keypoint Position Error (MPKPE), Velocity Distance (Vel-Dist) and Acceleration Distance (Acc-Dist). SR reflects the overall viability and stability of the policy; MPKPE respectively quantify the accuracy of keypoint tracking in the world coordinate frame; Vel-Dist quantifies the difference in joint velocities between the reference motion and the executed motion of the robot; Acc-Dist quantifies the difference in joint acceleration between the reference motion and the executed motion of the robot. For real-world evaluation, we deploy UniTracker on the Unitree G1 humanoid robot, which stands 1.3 meters tall and has 29 degrees of freedom. We control 23 DoFs by locking the 6 wrist joints.

#### B. Baselines

**What kind of motion tracker yields the best tracking performance?** We include two baselines: (1) a universal policy trained from scratch without the teacher-student architecture, and (2) a teacher-student framework using DAgger in the second stage without a CVAE. Direct comparisons with prior methods are not included, as their implementations are not publicly available. Experimental results in Table I show that UniTracker consistently outperforms both prior methods and our baselines across all evaluation metrics.

#### C. Ablation Studies

**Which dataset is most suitable for training a general motion tracker?** To assess the impact of training data quality, we compare two versions of the dataset: one filtered using PHC [23] and one unfiltered. The PHC-filtered dataset



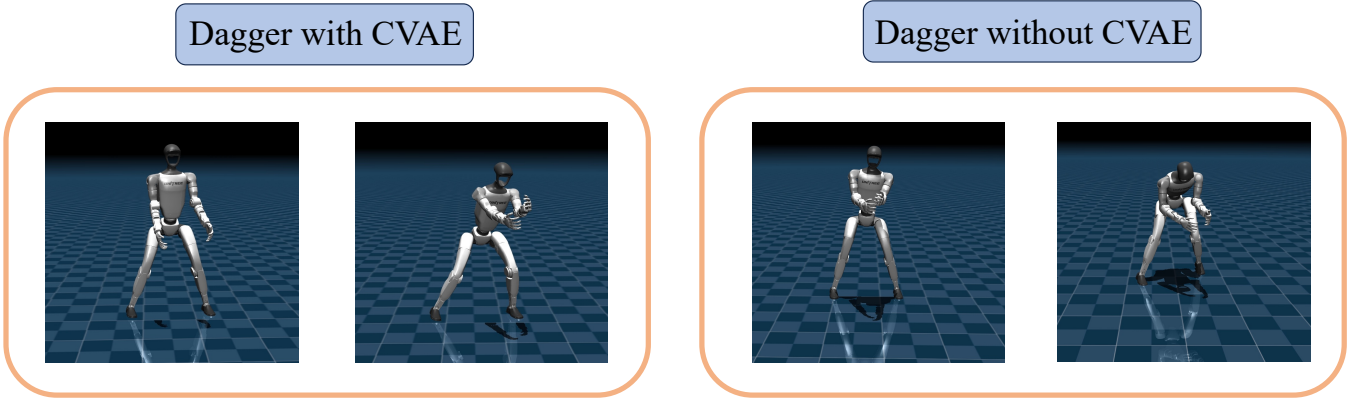


Fig. 3: The generalization capability of UniTracker in MuJoCo

removes highly aggressive motions that are physically infeasible for the robot. As a result, policies trained on this dataset tend to produce smoother and more stable motions. In contrast, the results in Figure 4 which training with the unfiltered dataset leads to a noticeable increase in keypoint tracking error, indicating that the policy struggles to follow the reference motions accurately. Moreover, we observe significantly higher action rates and velocity changes, suggesting that the learned policy exhibits overly aggressive behavior, making it unsuitable for deployment on real hardware.

**What model architecture best balances diversity, expressiveness and robustness?** To answer this question, we first investigated whether the RL actor (the decoder in the CVAE) should explicitly take the reference motion as part of its input. We evaluated two variants: one where the actor input is  $(s_t^{p-deploy}, s_t^{g-deploy}, z_t)$  and another where the reference motion is excluded. The results show that when the actor receives the reference motion directly, the influence of the latent variable  $z$  vanishes. In this case, the behavior of the model closely resembles that of a standard DAgger setup, as the strong reference input causes the policy to ignore the latent guidance. We further evaluated a pure DAgger setup with an MLP-based actor in the second stage. While this design performs well on motions seen during training, it degrades noticeably on out-of-distribution (OOD) motions. The strong reliance on explicit reference inputs reduces the policy’s robustness and its ability to generalize to unseen or novel motion sequences.

In Figure 3, we evaluate the generalization capability of UniTracker in MuJoCo by testing it on a challenging lateral squat motion, which demands strong balance control from the robot. Although UniTracker cannot precisely track all keypoints of the reference motion, it successfully produces a plausible lateral squat behavior while maintaining balance. In contrast, the DAgger baseline without the CVAE fails to remain stable and results in the robot falling, highlighting the importance of latent motion modeling for generalization to unseen motions.

In Table II, we evaluate the robustness of our policy by incrementally adding noise to the observations. In this table, a noise level of 0 indicates no observation noise, while higher

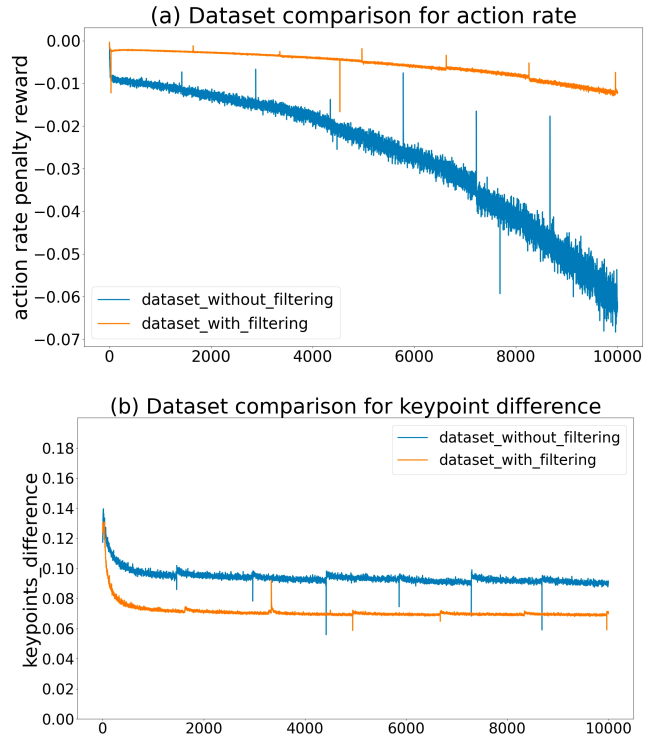
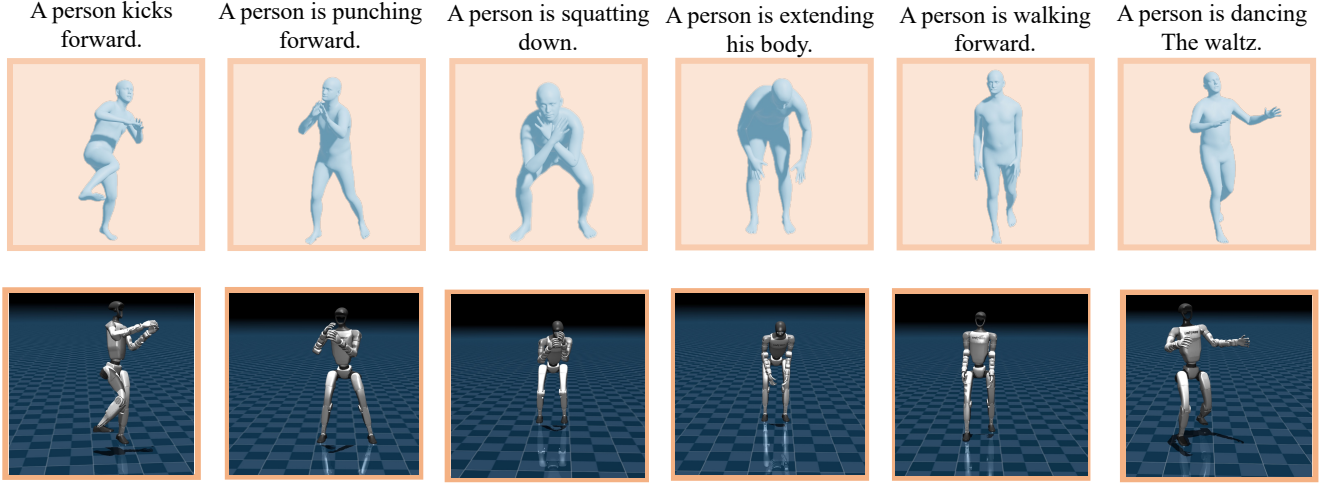


Fig. 4: The comparison of different datasets on action rate and keypoint difference

levels correspond to increasing noise intensity. We observe that UniTracker consistently outperforms the variant without CVAE in both Success Rate (SR) and Mean Per Keypoint Position Error (MPkPE). Moreover, UniTracker exhibits a slower degradation in performance as noise increases, indicating stronger robustness under observation perturbations.

**What hyperparameter choices lead to the best performance in whole-body motion tracking?** We conduct ablation studies on three key hyperparameters in our framework: the CVAE latent dimension, the future window size of the reference motion used in the CVAE prior, and the weight of the KL loss term. For the latent dimension, we experiment with values of 32, 64, 128, and 256. We observe that a dimension of 64 yields the best performance. Larger

## Text-to-Motion Generation



## Video-based Motion Estimation

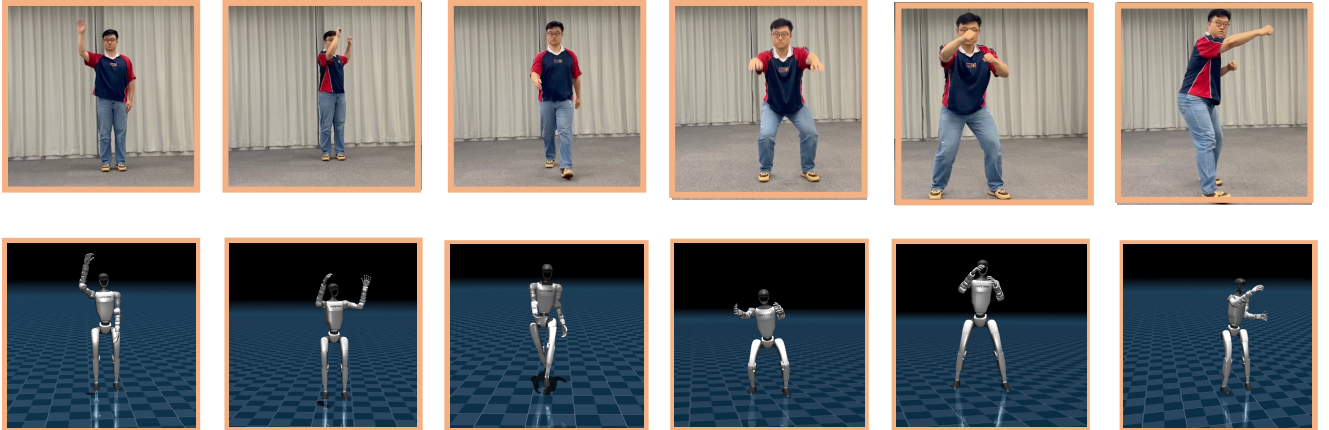


Fig. 5: **The Outcome of Downstream Applications in mujoco:** We evaluate text-to-motion generation and video-based motion estimation in the muJoCo simulator. The results demonstrate that our policy can effectively track both types of reference motions

latent sizes make the CVAE harder to train and do not lead to further improvements. Results are shown in Table I For the future window, which controls how many future frames of reference motion are included in the prior input, we test window sizes of 1, 5, 10, and 20 frames. The results indicate that using 5 future frames provides the best trade-off between responsiveness and stability. Lastly, we tune the KL loss coefficient with values of 1.0, 0.1, 0.01, and 0.001. We find that setting the weight to 0.1 leads to the best policy performance, effectively balancing latent regularization and reconstruction quality.

### D. Downstream Applications

We evaluate two downstream applications of our framework: motion generation and video-based motion estimation.

For motion generation, we use the MDM [26] model to produce SMPL-based [21] motion sequences conditioned on text input. These motions are then retargeted to the G1 humanoid robot for tracking. Both MuJoCo [27] simulation and real-world results demonstrate that our policy can accurately track motions generated from text prompts. For video estimation, we record a long motion sequence using a monocular camera, and convert it to SMPL format using GVHMR [28]. The resulting motion is retargeted to the G1 robot. Experiments in both MuJoCo and the real world show that our policy successfully tracks the reconstructed motions. These two applications highlight the strong generalization capability of our policy across different types of reference inputs.

Methods	All AMASS Train Dataset SR $\uparrow$	MPKPE $\downarrow$
(a) Noise Level 0		
Dagger without CVAE	88.21	84.79
Ours	<b>91.83</b>	<b>82.62</b>
(b) Noise Level 1		
Dagger without CVAE	85.79	88.65
Ours	<b>90.26</b>	<b>83.84</b>
(c) Noise Level 2		
Dagger without CVAE	79.58	93.71
Ours	<b>86.79</b>	<b>87.31</b>

TABLE II: We evaluate the robustness of the policy by incrementally adding noise to the observations. UniTracker consistently outperforms the variant without CVAE and exhibits a slower degradation in performance as the noise level increases.

#### IV. RELATED WORK

##### A. Whole-Body Controller for Humanoid Robots

Whole-body control is essential for enabling humanoid robots to perform a wide variety of complex tasks. Prior to the rise of reinforcement learning, researchers primarily relied on traditional optimization-based control methods for humanoid whole-body control [29–35]. These approaches typically required explicit mathematical modeling of both the robot and its environment, followed by real-time optimization to compute the robot’s next action. However, such methods often struggle to adapt to environmental variations, resulting in limited robustness. Additionally, they impose heavy computational demands during online execution.

To overcome these limitations, reinforcement learning (RL) has emerged as a powerful alternative, offering the ability to learn adaptive, robust control policies directly from interaction with the environment without relying on explicit modeling. Current reinforcement learning–based whole-body controllers for humanoid robots can be categorized by the source of their control signals, including teleoperation [1–6], offline motion datasets [7, 8, 10, 11], video-based motion estimation [13, 14] [5, 6], and high-level task commands [15, 16]. Teleoperation involves directly controlling the humanoid robot in real time using human input, often through motion capture systems or wearable sensors, allowing the robot to mimic human movements with high fidelity. Representative works in this area include Twist [1] and H2O [4], both of which adopt a two-stage teacher-student framework. The primary difference lies in the design of the policy’s observation space. Offline motion datasets consist of pre-collected human or humanoid motion sequences, which are used as references for training control policies through motion imitation. Representative works are Exbody [11] and Exbody2 [10], which begins by carefully curating an offline motion dataset and then decouples upper and lower-body motions as much as possible, aiming to maintain stability in the lower body while encourage diversity and expressiveness in the upper body. In

addition, the most recent work, GMT [12], is the first to demonstrate tracking of 8,000 motions using a single unified policy. Video-based motion estimation methods leverage visual input from videos to extract human motion data, which can then be used to guide humanoid robot control policies. This approach enables learning from large-scale, diverse motion sources without requiring direct human demonstration. A representative work is VideoMimic [13], which develops a real-to-sim-to-real pipeline to model both the robot and its surrounding environment. Task commands refer to high-level, sparse control signals that specify desired outcomes or goals, such as walking direction or target position, rather than detailed joint-level motions, enabling efficient whole-body control through abstraction. Representative works include Hover [15] and HugWBC [16]. Hover unifies multiple control modes into a single policy, enabling seamless transitions while retaining the strengths of each mode, thus providing a robust and scalable humanoid control solution. HugWBC designs a general task and behavior command space and employs techniques such as symmetrical loss and intervention training. This enables real-world humanoid robots to perform a variety of natural gaits—including walking, jumping, and hopping.

##### B. Environmental Adaption

Environment adaptation is essential for humanoid robots to maintain robust performance amid variations and uncertainties such as changes in terrain, external disturbances, or sensor noise in real-world conditions. One widely adopted approach to enhance environment adaptation is domain randomization (DR) [25]. By introducing randomized variations in simulation parameters such as physical properties, textures, lighting, and sensor noise during training, DR encourages the learned policy to generalize better and become more robust to real-world uncertainties without requiring explicit modeling of every possible scenario. Another approach to handling environmental adaptation is ASAP [9], which introduces a two-stage framework to bridge the dynamics gap between simulation and the real world for agile humanoid control. In the first stage, a motion tracking policy is trained in simulation. In the second stage, this policy is fine-tuned using a delta action model learned from real-world roll-out data. By compensating for simulation-to-reality discrepancies through residual actions, ASAP enables robust and expressive whole-body motions on real hardware, outperforming traditional approaches such as system identification and domain randomization.

#### V. CONCLUSION

In this work, we present UniTracker, a unified and robust whole-body motion tracking framework for humanoid robots. Unlike previous methods that either rely on strong reference condition or lack generalization capabilities, UniTracker leverages a CVAE-based policy architecture to balance motion expressiveness, policy robustness, and real-world deployability within a single, streamlined design. We conduct extensive experiments in simulation and on real hardware.



Name	Function
tracking keypoints	$\exp(\ p_t^{ref} - p_t\ )$
tracking joint position	$\exp(\ q_t^{ref} - q_t\ )$
tracking joint velocity	$\exp(\ \dot{q}_t^{ref} - \dot{q}_t\ )$
tracking body linear velocity	$\exp(\ \dot{p}_t^{ref} - \dot{p}_t\ )$
action rate	$-  a_t - a_{t-1}  $
torque	$-\tau$
slippage	$-  v_t^{foot} * F_t^{contact}  $

TABLE III: Definition of Reward Functions

Simulation results across multiple metrics show that UniTracker significantly outperforms our baselines. Real-world experiments on the Unitree G1 robot further confirm that our policy can track a wide range of motions—including walking, kicking, turning, dancing, and squatting—using a single general policy. Finally, we validate the generalization capabilities of UniTracker through two downstream applications: text-conditioned motion generation and video-based motion estimation, both of which demonstrate that our method can track external motion sources that were never seen during training. These results highlight UniTracker’s potential as a scalable and flexible solution for expressive whole-body humanoid control in the real world.

#### REFERENCES

- [1] Y. Ze *et al.*, *Twist: Teleoperated whole-body imitation system*, 2025. arXiv: 2505.02833 [cs.RO].
- [2] C. Lu *et al.*, *Mobile-television: Predictive motion priors for humanoid whole-body control*, 2025. arXiv: 2412.07773 [cs.RO].
- [3] Z. Fu, Q. Zhao, Q. Wu, G. Wetzstein, and C. Finn, *Humanplus: Humanoid shadowing and imitation from humans*, 2024. arXiv: 2406.10454 [cs.RO].
- [4] T. He *et al.*, *Learning human-to-humanoid real-time whole-body teleoperation*, 2024. arXiv: 2403.04436 [cs.RO].
- [5] R.-Z. Qiu *et al.*, *Humanoid policy human policy*, 2025. arXiv: 2503.13441 [cs.RO].
- [6] T. He *et al.*, *Omnih2o: Universal and dexterous human-to-humanoid whole-body teleoperation and learning*, 2024. arXiv: 2406.08858 [cs.RO].
- [7] Y. Shao *et al.*, *Langwbc: Language-directed humanoid whole-body control via end-to-end learning*, 2025. arXiv: 2504.21738 [cs.RO].
- [8] J. Shi *et al.*, *Adversarial locomotion and motion imitation for humanoid policy learning*, 2025. arXiv: 2504.14305 [cs.RO].
- [9] T. He *et al.*, *Asap: Aligning simulation and real-world physics for learning agile humanoid whole-body skills*, 2025. arXiv: 2502.01143 [cs.RO].
- [10] M. Ji *et al.*, *Exbody2: Advanced expressive humanoid whole-body control*, 2025. arXiv: 2412.13196 [cs.RO].
- [11] X. Cheng, Y. Ji, J. Chen, R. Yang, G. Yang, and X. Wang, *Expressive whole-body control for humanoid robots*, 2024. arXiv: 2402.16796 [cs.RO].
- [12] Z. Chen, M. Ji, X. Cheng, X. Peng, X. B. Peng, and X. Wang, “Gmt: General motion tracking for humanoid whole-body control,” *arXiv:2506.14770*, 2025.
- [13] J. Mao *et al.*, *Learning from massive human videos for universal humanoid pose control*, 2024. arXiv: 2412.14172 [cs.RO].
- [14] A. Allshire *et al.*, *Visual imitation enables contextual humanoid control*, 2025. arXiv: 2505.03729 [cs.RO].
- [15] T. He *et al.*, *Hover: Versatile neural whole-body controller for humanoid robots*, 2025. arXiv: 2410.21229 [cs.RO].
- [16] Y. Xue, W. Dong, M. Liu, W. Zhang, and J. Pang, *A unified and general humanoid whole-body controller for versatile locomotion*, 2025. arXiv: 2502.03206 [cs.RO].
- [17] S. Ross, G. J. Gordon, and J. A. Bagnell, *A reduction of imitation learning and structured prediction to no-regret online learning*, 2011. arXiv: 1011.0686 [cs.LG].
- [18] Unitree, *Unitree g1 humanoid agent ai avatar*, 2024.
- [19] J. Schulman, F. Wolski, P. Dhariwal, A. Radford, and O. Klimov, *Proximal policy optimization algorithms*, 2017. arXiv: 1707.06347 [cs.LG].
- [20] N. Mahmood, N. Ghorbani, N. F. Troje, G. Pons-Moll, and M. J. Black, *Amass: Archive of motion capture as surface shapes*, 2019. arXiv: 1904.03278 [cs.CV].
- [21] M. Loper, N. Mahmood, J. Romero, G. Pons-Moll, and M. J. Black, “SMPL: A skinned multi-person linear model,” *ACM Trans. Graphics (Proc. SIGGRAPH Asia)*, vol. 34, no. 6, 248:1–248:16, Oct. 2015.
- [22] X. B. Peng, P. Abbeel, S. Levine, and M. van de Panne, “Deepmimic: Example-guided deep reinforcement learning of physics-based character skills,” *ACM Transactions on Graphics*, vol. 37, no. 4, pp. 1–14, Jul. 2018.
- [23] Z. Luo, J. Cao, A. Winkler, K. Kitani, and W. Xu, *Perpetual humanoid control for real-time simulated avatars*, 2023. arXiv: 2305.06456 [cs.CV].
- [24] V. Makovychuk *et al.*, *Isaac gym: High performance gpu-based physics simulation for robot learning*, 2021. arXiv: 2108.10470 [cs.RO].
- [25] J. Tobin, R. Fong, A. Ray, J. Schneider, W. Zaremba, and P. Abbeel, *Domain randomization for transferring deep neural networks from simulation to the real world*, 2017. arXiv: 1703.06907 [cs.RO].

- [26] G. Tevet, S. Raab, B. Gordon, Y. Shafir, D. Cohen-Or, and A. H. Bermano, *Human motion diffusion model*, 2022. arXiv: 2209.14916 [cs.CV].
- [27] E. Todorov, T. Erez, and Y. Tassa, “Mujoco: A physics engine for model-based control,” in *2012 IEEE/RSJ International Conference on Intelligent Robots and Systems*, IEEE, 2012, pp. 5026–5033.
- [28] Z. Shen *et al.*, “World-grounded human motion recovery via gravity-view coordinates,” in *SIGGRAPH Asia Conference Proceedings*, 2024.
- [29] L. Sentis and O. Khatib, “A whole-body control framework for humanoids operating in human environments,” in *Proceedings 2006 IEEE International Conference on Robotics and Automation, 2006. ICRA 2006.*, 2006, pp. 2641–2648.
- [30] M. Chignoli, D. Kim, E. Stanger-Jones, and S. Kim, *The mit humanoid robot: Design, motion planning, and control for acrobatic behaviors*, 2021. arXiv: 2104.09025 [cs.RO].
- [31] S. Kuindersma *et al.*, “Optimization-based locomotion planning, estimation, and control design for the atlas humanoid robot,” English, *Autonomous Robots*, vol. 40, no. 3, pp. 429–455, Mar. 2016.
- [32] J. Li and Q. Nguyen, *Dynamic walking of bipedal robots on uneven stepping stones via adaptive-frequency mpc*, 2022. arXiv: 2209.08664 [cs.RO].
- [33] E. Westervelt, J. Grizzle, and D. Koditschek, “Hybrid zero dynamics of planar biped walkers,” *IEEE Transactions on Automatic Control*, vol. 48, no. 1, pp. 42–56, 2003.
- [34] B. Dariush, M. Gienger, B. Jian, C. Goerick, and K. Fujimura, “Whole body humanoid control from human motion descriptors,” in *2008 IEEE International Conference on Robotics and Automation*, 2008, pp. 2677–2684.
- [35] S. Kajita, F. Kanehiro, K. Kaneko, K. Yokoi, and H. Hirukawa, “The 3d linear inverted pendulum mode: A simple modeling for a biped walking pattern generation,” in *Proceedings 2001 IEEE/RSJ International Conference on Intelligent Robots and Systems. Expanding the Societal Role of Robotics in the the Next Millennium (Cat. No.01CH37180)*, vol. 1, 2001, pp. 239–246 vol.1.